Journal of Pharmaceutical Analysis 14 (2024) 100952

Contents lists available at ScienceDirect

Journal of Pharmaceutical Analysis

journal homepage: www.elsevier.com/locate/jpa

Original article

An Fe–Cu bimetallic organic framework as a microwave sensitizer for treating tumors using combined microwave thermotherapy and chemodynamic therapy

Xinyang Zhu [a, b], Chao He [b], Longfei Tan [c], Xun Qi [a], Meng Niu [a], Xianwei Meng [c], Hongshan Zhong [a, *]

[a] Department of Key Laboratory of Diagnostic Imaging and Interventional Radiology of Liaoning Province, The First Affiliated Hospital of China Medical University, Shenyang, 110001, China
[b] Xixian New Area Rimag Medical Diagnosis Center, Second Affiliated Hospital of Shaanxi University of Chinese Medicine, Xianyang, Shaanxi, 712099, China
[c] Laboratory of Controllable Preparation and Application of Nanomaterials, Laboratory of Cryogenics, Technical Institute of Physics and Chemistry, Chinese Academy of Sciences, Beijing, 100190, China

ARTICLE INFO

Article history:
Received 15 September 2023
Received in revised form
18 January 2024
Accepted 19 February 2024
Available online 27 February 2024

Keywords:
Microwave thermotherapy
Metal organic frameworks
Glutathione scavenging
Magnetic resonance imaging
Synergism

ABSTRACT

Microwave thermotherapy (MWTT), as a treatment for tumors, lacks specificity and requires sensitizers. Most reported microwave sensitizers are single metal-organic frameworks (MOFs), which must be loaded with ionic liquids to enhance the performance in MWTT. Meanwhile, MWTT is rarely combined with other treatment modalities. Here, we synthesized a novel Fe–Cu bimetallic organic framework FeCuMOF (FCM) by applying a hydrothermal method and further modified it with methyl polyethylene glycol (mPEG). The obtained FCM@PEG (FCMP) showed remarkable heating performance under low-power microwave irradiation; it also acted as a novel nanospheres enzyme to catalyze H_2O_2 decomposition, producing abundant reactive oxygen species (ROS) to deplete glutathione (GSH) and prevent ROS clearance from tumor cells during chemodynamic treatment. The FCMP was biodegradable and demonstrated excellent biocompatibility, allowing it to be readily metabolized without causing toxic effects. Finally, it was shown to act as a suitable agent for T_2 magnetic resonance imaging (MRI) *in vitro* and *in vivo*. This new bimetallic nanostructure could successfully realize two tumor treatment modalities (MWTT and chemodynamic therapy) and dual imaging modes (T_2 MRI and microwave thermal imaging). Our findings represent a breakthrough for integrating the diagnosis and treatment of tumors and provides a reference for developing new microwave sensitizers.

1. Introduction

Hepatocellular carcinoma (HCC) is characterized by a high degree of malignancy, high recurrence and metastasis rates, and a low survival rate [1–3]. Existing treatment methods, including conventional surgery, radiotherapy, and chemotherapy, are not sufficiently effective. Emerging treatment methods, such as microwave thermotherapy (MWTT), kill tumor cells by applying heat to damage their cell membranes, thereby halting the synthesis of biomolecules and inhibiting cell proliferation, ultimately leading to tumor tissue necrosis [4,5]. MWTT offers several advantages over traditional treatments, including ease of operation, minimal side effects, and deep tissue penetration [6–8]; however, it also comes with some disadvantages in clinical tumor treatment. First, as an invasive procedure, MWTT carries surgical risks and local side effects. Second, this treatment lacks sensitivity and specificity [9]. High microwave power could harm adjacent normal tissue and vital organs, while low power may not achieve the desired tumor inhibition.

To address these issues, a noninvasive thermotherapy method mediated by a microwave sensitizer was introduced. Currently, the most popular microwave sensitizers are single-metal organic frameworks (MOFs) composed of a metal compound and its corresponding ligands [10–16]. Leveraging the enhanced permeability and retention effect of tumor tissue [17,18], MOFs can accumulate at the tumor site and achieve remarkable heating under low-power

* Corresponding author.
E-mail address: hszhong@cmu.edu.cn (H. Zhong).

https://doi.org/10.1016/j.jpha.2024.02.006

microwave irradiation, simultaneously inhibiting the tumor and preserving normal tissue [19,20]. Unfortunately, most microwave sensitizers currently in use require the loading of ionic liquids to enhance their heating performance, making the synthesis more complex, leading to product aggregation, and reducing heating efficiency. Due to factors such as the complex tumor structure, the unique tumor microenvironment, and high rates of recurrence and metastasis, the effectiveness of MWTT alone in tumor inhibition is limited. Therefore, there is a need to synergize the MWTT with other treatment methods to enhance the tumor-suppressive effect.

Reactive oxygen species (ROS) can destroy tumor cell structures, inhibiting tumor tissue growth in chemodynamic therapy (CDT) [21]. Consequently, the combination of MWTT and CDT using a single microwave sensitizer holds promise for enhancing the antitumor effect. It has been reported that the tumor microenvironment is enriched with glutathione (GSH) [22,23], which scavenges ROS and compromises the efficacy of CDT. Therefore, it is highly desirable to develop new MOFs that not only demonstrate synergy between MWTT and CDT but also eliminate GSH and enhance the efficiency of CDT [24–26]. Mn-doped metal-organic framework (Mn-ZrMOF) nanocubes have been reported to achieve synergy between MWTT and dynamic therapy [27].

Taking inspiration from the research on Mn-ZrMOF nanocubes, we designed and synthesized a new biodegradable bimetallic organic framework, FeCuMOF (FCM), and modified its surface with poly(ethylene glycol) (PEG) to enhance its biocompatibility. We abbreviate the obtained material as FCM@PEG or FCMP (Scheme 1). Subsequently, we conducted *in vitro* microwave heating experiments to investigate the microwave heating effect of FCMP nanospheres under low-power microwave irradiation. Because FCMP has been shown to catalyze the generation of •OH from H_2O_2 [28], we studied the amount of •OH generated under similar reaction conditions. Furthermore, FCMP exhibits *in vivo* and *in vitro* T_2 magnetic resonance imaging (MRI) performance due to its internal metal iron ions [29,30], suggesting its potential value in T_2 MRI-mediated tumor therapy. Consequently, we performed *in vivo* tumor inhibition experiments to demonstrate the ability of FCMP nanospheres to inhibit tumors. Our results contribute to advancements in tumor diagnosis and treatment and foster research and development in the field of new microwave sensitizers.

2. Materials and methods

2.1. Materials

Terephthalic acid (H2BDC), 2-aminoterephthalic acid (H2BDC-NH_2), and $FeCl_3$ were purchased from Bellingway Fine Materials Chemical Reagent Co., Ltd. (Beijing, China). Cupric nitrate

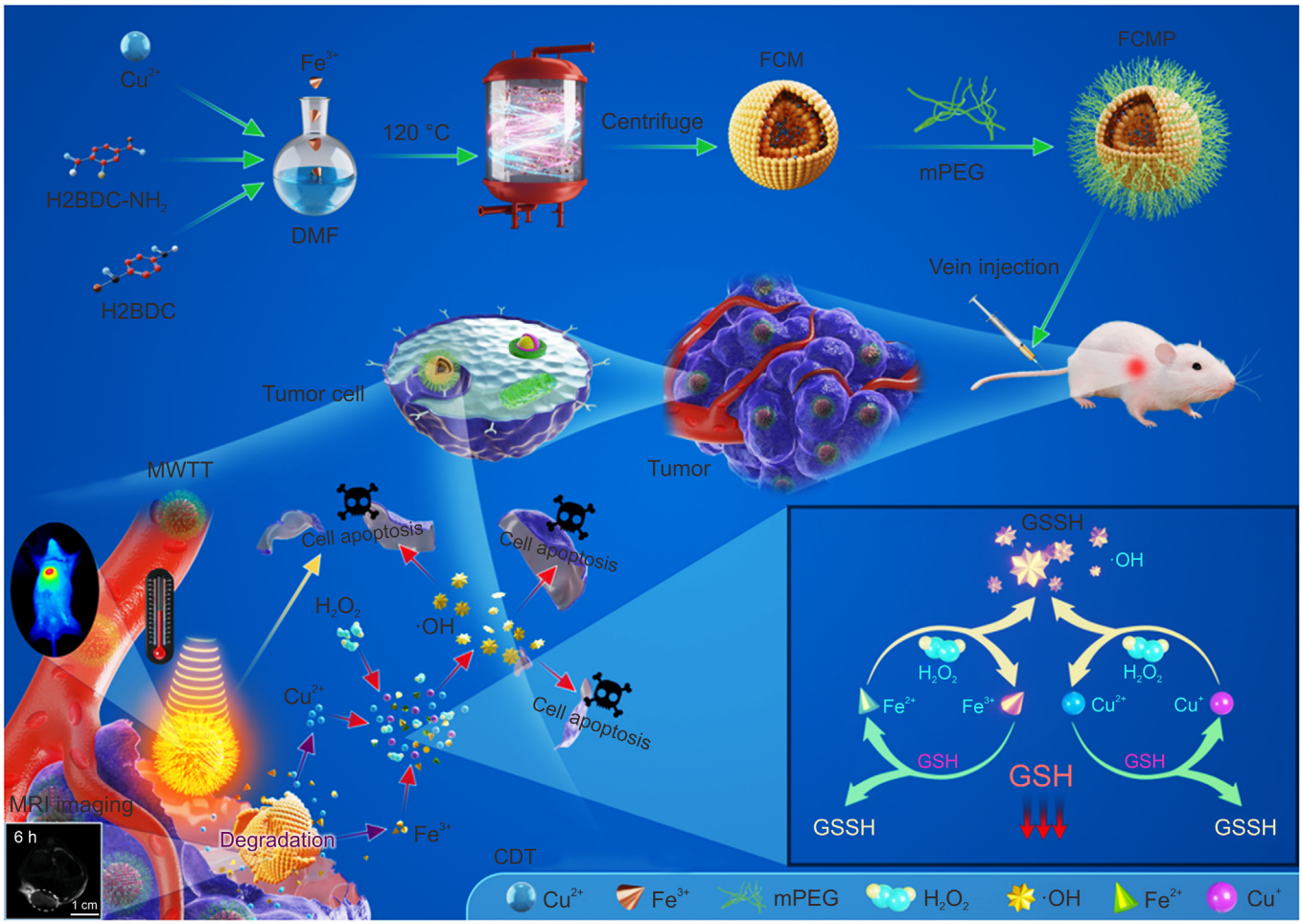

Scheme 1. The synthesis of Fe–Cu metal organic framework (FCM)@poly(ethylene glycol) (PEG) (FCMP) and its inhibition of tumors via microwave thermotherapy (MWTT) and chemodynamic therapy (CDT). First, the schematic illustration shows the synthesis process of multifunctional FCMP nanospheres by a hydrothermal method, followed by surface modification with methyl PEG (mPEG). When FCMP was injected, it accumulated in tumor tissue, was quickly degraded, released ions, and produced •OH. Under microwave irradiation, the temperature increased significantly, achieving the combined effects of MWTT and CDT and inhibition of the tumor growth. H2BDC-NH_2: 2-aminoterephthalic acid; H2BDC: terephthalic acid; DMF: *N*,*N*-dimethylformamide; GSH: glutathione; GSSH: oxidized GSH.

hexahydrate was purchased from Yongda Chemical Reagent Co., Ltd. (Tianjin, China). PEG was obtained from Kaizheng United Technology Co., Ltd. (Beijing, China). 2,7-dichlorofluorescein acetoacetic acid (DCFH-DA) was purchased from Shanghai Biyuntian Biotechnology Co., Ltd. (Shanghai, China). *N*,*N*-dimethylformamide (DMF) was obtained from Concord Co., Ltd. (Beijing, China). 3,3,5,5-tetramethylbenzidine (TMB) and 5,5′-dithio-bis-(2-nitrobenzoic acid) (DTNB) were provided by Solar Energy Co., Ltd. (Beijing, China). The above reagents were of analytical grade and needed no further processing or refining.

2.2. Animals

Animal experiments were carried out following the Guide for the Care and Use of Laboratory Animals (8th edition) and were approved by the Animal Ethics Committee of the First Clinical College of China Medical University (CMU) (Approval No.: CMUXN202 1711). All experiments were conducted at the Animal Center of CMU. Male Kunming mice (4–5 weeks old) were randomly allocated according to the experimental design. The tumor-bearing mice were established by subcutaneous injection of hepatoma cells (H22, approximately 10^7 per mouse) in the right upper abdomen area. After seven days, tumor suppression experiments were performed.

2.3. Preparation of FCM

Copper nitrate hexahydrate (100 mg), H2BDC (50 mg), H2BDC-NH_2 (35 mg), and $FeCl_3$ (150 mg) were sequentially added to 100 mL of DMF and ultrasonically mixed for several minutes. The mixed solution was transferred into a clean kettle, which was then sealed and kept in a closed dry oven for 12 h at 120 °C. After cooling for 3–4 h, the solid product FCM was washed with anhydrous ethanol and centrifuged several times before storage.

2.4. Preparation of FCMP

Methoxy-polyethylene glycol sulfhydryl (mPEG-SH) (20 mg) and FCM (40 mg) were dissolved in 4 and 20 mL, respectively, of deionized water and ultrasonically dispersed. The mPEG-SH solution was dropped into the FCM solution, which was magnetically stirred for 6 h. Then, the mixed solution was centrifuged and washed four times to obtain the bimetallic framework FCMP in the form of nanospheres.

2.5. In vitro heating of FCMP under microwave irradiation

The microwave heating performance of FCMP nanospheres at different concentrations was examined using *in vitro* experiments. A given amount of FCMP (0, 1, 3, 5, and 10 mg) was uniformly dispersed in saline, placed in a container, and irradiated with microwave (1.8 W) for 5 min. Plain saline was used as a control. Real-time infrared (IR) thermography was used to record the medial temperature in the container every 10 s, and the data were used for drawing the heating curves.

2.6. In vitro GSH clearance test

To evaluate the ability of FCMP to scavenge GSH *in vitro*, different amounts of FCMP nanospheres (0, 1, 2, 3, 4, 5, and 6 mg) were dissolved in deionized water and reacted with GSH (10 mM) for 20 min. After centrifuging the reaction mixture, the supernatant was collected. Separately, an FCMP solution of fixed concentration was reacted with GSH, and the supernatant was collected by centrifugation after different reaction times (10, 20, 40, and 80 min). To measure the GSH content, the supernatant was mixed with deionized water, DTNB, and phosphate-buffered saline (PBS) solution (pH 7.4) for a few minutes. Then, the absorption peak of GSH was measured using an ultraviolet (UV) spectrophotometer in the range of 405–500 nm to assess the ability of FCMP to scavenge GSH at different concentrations and reaction times.

At the cellular level, we incubated H22 cells with FCMP solutions at different concentrations for 24 h. Then, the cells were analyzed according to the instructions of the GSH kit (BC1175; Solarbio, Beijing, China). The absorption peak of GSH at 412 nm was detected, and the percentage of residual GSH in the cells was calculated.

2.7. In vitro chemodynamic therapy with FCM/FCMP

As an index for efficacy in CDT, we used the TMB method to measure and evaluate the ability of FCM nanospheres to produce •OH at different concentrations and reaction times. We compared three types of MOF nanospheres: the single MOFs FeMOF (FM), CuMOF (CM), as well as bimetallic FCM. First, a given amount of the MOF material was dispersed in deionized water. The TMB solution was obtained by dissolving TMB powder (30 mg) into dimethyl sulfoxide (DMSO) (3 mL). For the time-dependent measurement, the TMB solution (20 μL) and 1% H_2O_2 were added to the MOF dispersion and reacted for different times (1, 3, 5, 7, 9, 11, 13, and 15 min). Then, an UV-visible (UV-vis) spectrophotometer was used to measure absorption in the range of 525–775 nm. To measure the dose effect, a certain concentration of the MOF material (1–5 μg/mL) was subjected to the same reaction conditions for 10 min (other conditions remained the same), and the UV absorption was measured. We further plotted absorption curves at 652 nm for each material at different concentrations and reaction times. In addition to the absorbance, photographs were taken at the same amount of MOF material after 10 min of reaction. The color changes served as indicators of the abilities of FM, CM, and FCM to produce •OH.

To assess ROS production by FCMP at the cellular level, HCC cells were placed on a 12-well plate and divided into four groups: control, FCMP, H_2O_2, and H_2O_2 + FCMP. The cells in the control group were incubated in pure medium, while those in the latter three groups were incubated for 5 h with FCMP (100 μg/mL) and/or H_2O_2 (1%). Then, the cells in each group were incubated with medium containing DCFH-DA for 30 min and washed. These cells were examined and photographed under a fluorescence microscope.

2.8. MRI experiments in vitro and in vivo

The FCMP nanospheres were dispersed in deionized water at 0, 0.375, 0.75, 1.5, 3, 6, and 12 mg/mL and placed in a centrifuge tube. The tube was inserted into a glass dish containing agarose for complete solidification. Subsequently, MRI (3.0 T, T_2-weighted image (T_2WI)) was used to observe changes in the T_2 signal and verify whether FCMP could function in MRI *in vitro*.

In the corresponding *in vivo* experiment, FCMP solution (75 mg/kg) was injected into the tail veins of tumor-bearing mice of similar weight and tumor size. We performed MRI sequence T_2WI imaging before injection and at 3 and 6 h after injection. By comparing the changes in the T_2 signal in the tumor tissues, we evaluated the MRI performance of FCMP nanospheres in this mouse model.

2.9. Degradation of FCMP in vitro

The biodegradability of FCMP nanospheres was examined *in vitro* under neutral pH (pH 7.4), and it was also examined in an acidic buffer solution (pH 5.5) that was meant to simulate the tumor environment. The nanospheres were dispersed in centrifuge tubes at the same volume and different pH values. Then, the tubes

were sealed and kept in a 37 °C oscillator for different times (6, 12, or 24 h), and the solid was separated by centrifugation. The precipitates were dispersed in absolute ethyl alcohol and examined by transmission electron microscopy (TEM) to confirm the biodegradability of FCMP.

2.10. In vitro cellular uptake of FCMPs

We incubated HepG2 cells with FCMP nanospheres (100 μg/mL) for 12 h. The cells were collected, digested, and placed in centrifuge tubes, and fixed with 2.5% glutaraldehyde for several hours. This step was followed by cleaning, fixing, rinsing, dehydration, saturation, embedding, sectioning, and staining. Finally, the sample was placed on a copper net and observed through TEM to analyze FCMP uptake by tumor cells.

2.11. In vitro toxicity test of FCMP

We performed a methylthiazolyldiphenyl-tetrazolium (MTT) assay to evaluate the toxicity of different concentrations of FCMP on normal (L929) and hepatoma cells (H22 and HepG2 cells). These three types of cells were seeded in 96-well plates and incubated for 24 h. Then, FCMP was added at different concentrations to the wells for 24 h. Then, MTT solution (5%, 20 μL) was dripped into each well for 4 h. The liquid in the well was removed using a syringe, and DMSO (150 μL) was added. After the purple crystals in the well were completely dissolved, the absorbance value at 492 nm was measured using a microplate analyzer to calculate the cell survival rate. The above experiments were all carried out at least three times.

2.12. Animal acute toxicity test of FCMP

The health effects of different concentrations of FCMP nanospheres were assessed by performing acute toxicity tests in mice. Twenty healthy male Kunming mice (25 ± 1.5 g) were randomly divided into five groups and injected with different amounts of FCMP (0, 25, 50, 75, and 100 mg/kg) through the tail vein. Mice in the control group were injected with saline solution. Afterward, the mice were weighed and monitored daily. After 14 days, blood samples were collected from the mice and subjected to routine and blood biochemical tests. The important organs were collected and soaked in a 4% polyformaldehyde solution for 24 h. The morphology of the organs was observed using microscope photography after hematoxylin and eosin (H&E) staining. The results were used to evaluate the toxicity and safety of FCMP in mice.

2.13. In vitro antitumor experiment using combined treatments

To examine the efficacy of FCMP nanospheres in inhibiting tumor cells under combined MWTT and CDT, a suspension of H22 cells was added evenly to a six-well plate and incubated overnight. The cells were divided into control, H_2O_2, FCMP, and FCMP + H_2O_2 groups. The added concentrations of reagents were 100 μg/mL for FCMP and 50 μM for H_2O_2. The control group volume was made equal with Dulbecco's modified Eagle's medium (DMEM). After incubation for 24 h, the cells were resuspended in 1 mL culture solution. Then, microwave irradiation was performed at a power of 1.8 W for 0, 1, 3, and 5 min. The microwave-treated cells were placed on a 96-well plate and incubated overnight. Then, MTT (5%, 10 μL) was added to each well, and they were measured using a multifunctional enzyme standard instrument (BioTek, Beijing, China) to further calculate the tumor cell survival rate following different therapies.

2.14. In vitro cell migration test of FCMP

The inhibitory effect of FCMP nanospheres on tumor cell migration was evaluated using *in vitro* cell migration experiments. Tumor cells were incubated in simple culture medium (control) or treated with H_2O_2, FCMP, microwave, FCMP + H_2O_2, or FCMP + H_2O_2 + microwave. After 24 h, the cells were resuspended in culture medium containing 1% serum. The suspended cells were carefully moved to the upper compartment of the transwell system, and medium containing 20% serum was added to the lower compartment. The solution was removed after 18 h of incubation, and the inner cells in the upper compartment were gently removed and washed with PBS. Subsequently, the chamber was fixed with polyformaldehyde (4%) for 30 min, soaked in crystal violet solution for 30 min, washed with PBS many times, and observed and photographed under a microscope (Olympus, Tokyo, Japan).

2.15. In vitro cell apoptosis test of FCMP

Flow cytometry was used to examine the effect of FCMP nanospheres on tumor cell apoptosis. The groupings were identical to the cell migration experiment. The treated cells and the control cells were collected in centrifuge tubes and resuspended in specific buffer solution. To each sample, we simultaneously added fluorescein isothiocyanate (FITC; 5 μL) and propidium iodide (PI) staining solution (5 μL). The reaction was carried out for 15 min. Then, 400 μL of buffer solution was added to the sample tubes. Cell apoptosis was measured using a flow detector.

2.16. In vitro cell proliferation test of FCMP

Inhibition of tumor cell proliferation by different treatments was examined using the 5-ethynyl-2′-deoxyuridine (EdU) proliferation assay. The cells were seeded overnight in a 24-well plate and treated according to the assigned experimental group. Subsequently, the cells were processed using the method described in the instructions of the EdU test kit (UElandy Biotechnology, Suzhou, China). Finally, the doubly stained cells were observed and photographed under a fluorescence microscope (Olympus). The blue light of Hoechst was used to label all cells, and the red fluorescence of EdU represents cells with proliferative capacity. The merged image shows the cell proliferation ability of each experimental group. The viable cells in each group were counted under the corresponding field of vision to estimate the changes in cell proliferation ability.

2.17. In vivo tumor inhibition experiment

The antitumor effect of FCMP nanospheres in combination therapy was evaluated using tumor-bearing mice ($n = 20$, body weight 30 ± 2 g, tumor diameter 0.8 ± 0.05 cm). The mice were randomly divided into four groups (control, FCMP, microwave, and FCMP + microwave, $n = 5$ for each group). Mice in the FCMP and FCMP + microwave groups were given 200 μL of FCMP nanospheres (75 mg/kg), while the control and microwave groups were injected with normal saline of the same volume. Six hours after injection, the microwave and FCMP + microwave groups were irradiated with microwaves (1.8 W, 5 min) at the tumor site. During irradiation, temperature changes were detected and recorded by an IR thermal imager (Hikvision, Hangzhou, China) at the tumor site. After treatment, the body weight, tumor size, and survival of the mice were observed every day. Fourteen days later, the spleen, lungs, kidneys, heart, liver, and tumor tissues of the mice were harvested, photographed, and weighed. The obtained organs and tissues were cleaned with PBS and soaked in a liquid containing paraformaldehyde for internal fixation. After 24 h, these tissues

were embedded, sliced, and stained with H&E and terminal deoxynucleotidyl transferase dUTP nick-end labeling (TUNEL) fluorescence. The morphology and staining of tissue were observed under a microscope (Olympus), and the collected images were analyzed.

3. Results and discussion

3.1. Synthesis and characterization of FCM/FCMP nanospheres

The morphology and structure of FCM and FCMP nanospheres were observed using TEM and scanning electron microscopy (SEM). Figs. 1A and B show the TEM images of FCM and FCMP, and Figs. 1C and D show the SEM images of FCM and FCMP, respectively. The FCM and FCMP nanospheres had a round solid structure, regular shape, good dispersity, and uniform size. The zeta potentials of FCM and FCMP were 45.3 and −10.2 mV, respectively (Fig. 1E), and these values changed after loading mPEG. The average particle size of FCMP was 129.8 ± 21.9 nm (Fig. S1), and that of FCM was 87 ± 12.23 nm (Fig. 1F). The larger particle size of FCMP (Fig. 1F) verifies the successful loading of mPEG on FCM. Fig. 1G shows the high-resolution TEM image and the elemental mapping of FCMP nanospheres. The nanospheres contain abundant Fe, Cu, C, O, and Cl elements with even spatial distributions. In the spectra of Fig. S2, the percentages of different elements are indicated. The most abundant element was C (59.43%), followed by Cu (19.85%) and then Fe (8.31%), suggesting that the bimetallic organic frame structure FCMP was synthesized. Fourier transform infrared (FT-IR) spectroscopy was used to examine the functional groups of FCM, mPEG, and FCMP. In Fig. 1H, the strong and wide absorption bands between 3,250 and 3,650 cm^{-1} correspond to the O—H stretching vibration. The characteristic peak at 1,050 cm^{-1} belongs to C—O single bond stretching. FCMP and FCM also show nearly coinciding peaks at 3,410 and 1,396 cm^{-1}, suggesting that the amino group and benzene ring in the MOF remained intact after mPEG modification. We conducted X-ray diffraction (XRD) analysis and specific surface detection of the Fe—Cu bimetallic MOF. It is further shown that FCMP belongs to the MOF structure. The results are shown in Fig. S3. These results support the successful synthesis of FCMP nanospheres.

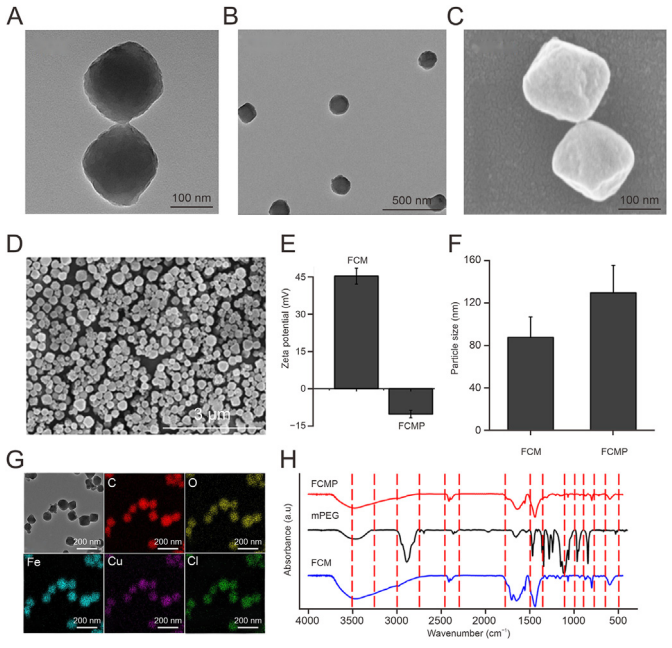

Fig. 1. Characterization of FeCuMOF (FCM)@polyethylene glycol (PEG) (FCMP) nanospheres. (A, B) Transmission electron microscope (TEM) images of FCM (A) and FCMP (B). (C, D) Scanning electron microscope (SEM) images of FCM (C) and FCMP (D). (E) Zeta potentials of FCM and FCMP. (F) Hydrodynamic diameters of FCM and FCMP. (G) High-resolution transmission electron microscopy image of FCMP and elemental mapping results for Fe, Cu, C, O, and Cl. (H) Fourier transform infrared (FT-IR) spectra of FCM, methyl PEG (mPEG), and FCMP.

3.2. In vitro heating performance under microwave irradiation

From the *in vitro* heating results, the solution temperature increased in the presence of FCMP, and the effect became stronger at higher FCMP concentrations and longer irradiation times (Fig. 2A). The corresponding IR thermal image also appeared brighter (Fig. 2B). The maximum temperature of 56.6 °C was reached at an FCMP concentration of 10 mg/mL, and the image became crimson in color. Fig. 2C compares the temperature changes after microwave irradiation. When the FCMP concentrations were 0, 1, 3, 5, and 10 mg, the final temperature increases were 16.9, 21.0, 23.3, 24.7, and 31.1 °C, respectively. At the maximum dosage (10 mg/mL), the temperature increase was 14.2 °C higher than that of the control. Therefore, the heating performance under microwaves is positively correlated with the concentration of FCMP nanospheres and the irradiation time.

3.3. In vitro GSH clearance performance

The GSH absorption peak gradually decreased with increasing FCMP mass. After adding the largest amount of FCMP (6 mg), the UV absorption at 405 nm was reduced from 1.66 to 0.22, indicating that 88% of the total GSH was consumed (Figs. 2D and S4). Subsequently, we treated 4 mg of FCMP with GSH for different time periods. After 10, 20, 40, and 80 min of reaction, the GSH absorption continuously decreased, reaching a final value of 0.36 after 80 min (78% GSH removal) (Fig. 2E). These results show that FCMP can efficiently scavenge GSH in a dose-dependent manner and that GSH clearance also increases with reaction time.

When we further tested the efficacy of FCMP in eliminating GSH from tumor cells, we found that the intracellular GSH level gradually decreased with increasing FCMP concentration. At 200 μg/mL, the GSH level decreased to 46.88% of the original value (Fig. 2F). Therefore, FCMP is also capable of clearing GSH from inside tumor cells in a dose-dependent manner.

3.4. In vitro performance in chemodynamic therapy

Our *in vitro* experiment using TMB revealed that FCM produces abundant •OH in the presence of H_2O_2; even a small amount of FCM has significant catalase-like activity. When •OH reacts with TMB, the latter is converted to oxidized TMB, which is blue in color and has a characteristic absorption peak at 652 nm. This reaction was used to further compare the •OH generation capacity of bimetallic FCM and monometallic FM and CM. As shown in Figs. 3A—C, as the mass of the MOF material increased, •OH production also increased. The FCM showed much higher •OH production than FM and CM. We also monitored the amount of •OH generated by the three MOFs at the same mass after different reaction times. In all cases, •OH production increased with the reaction time to various degrees (Figs. 3D—F), and FCM again showed the best performance. To better visualize the •OH production performance, we plotted the absorption peak at 652 nm as a function of MOF mass and reaction time (Figs. 3G and H). At a dosage of 15 μg, FCM produced 2.17- and 5.12-fold higher amounts of •OH than FM and CM, respectively. The photographs in Fig. 3I also confirm that the solution after the reaction was bluer for FCM (dark blue) than for the other groups. These results show that FCM has a significant advantage over FM and CM in •OH generation. Because of the higher amount of metal

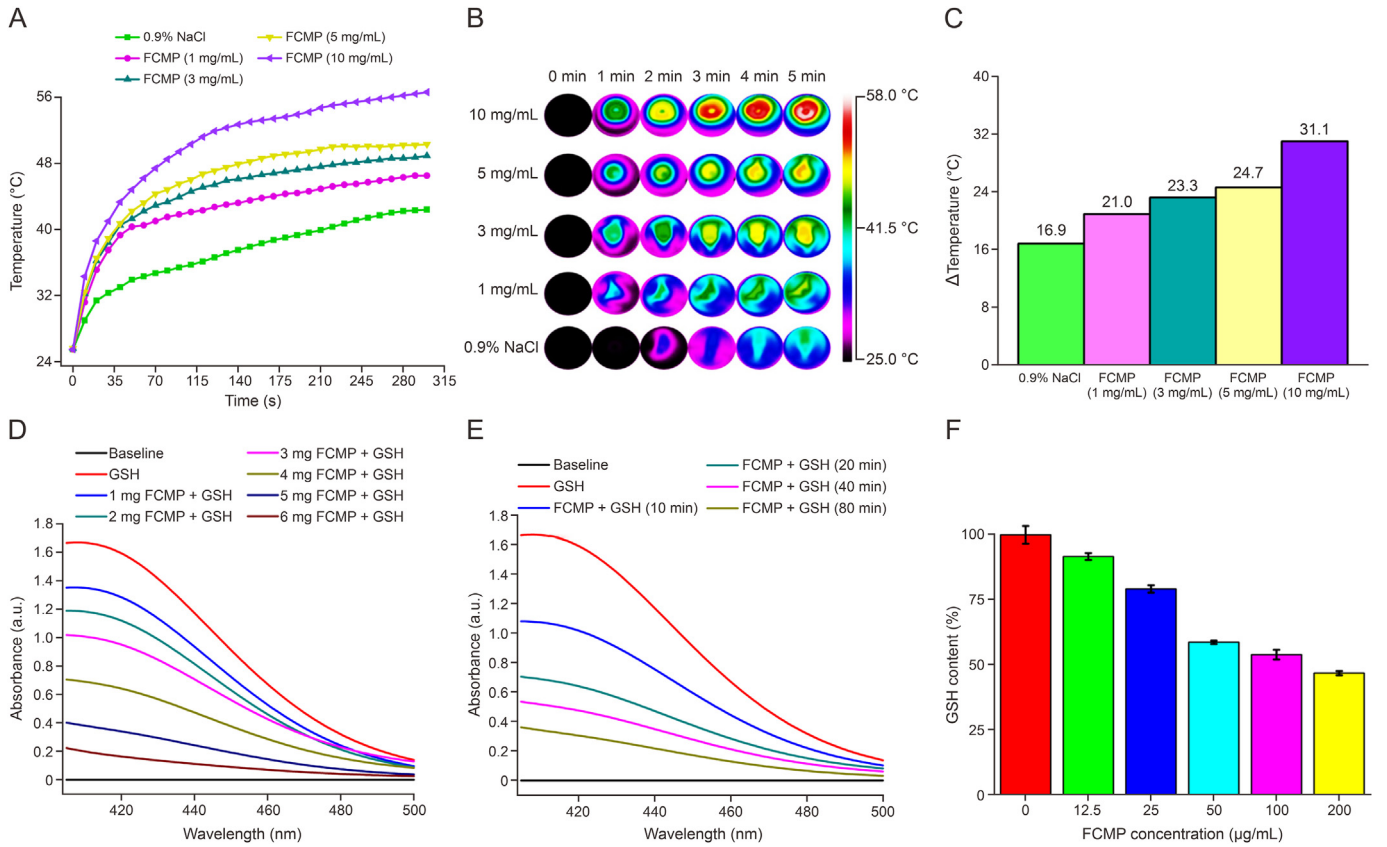

Fig. 2. Microwave thermotherapy (MWTT) and glutathione (GSH) scavenging performance of FeCuMOF (FCM)@polyethylene glycol (PEG) (FCMP) *in vitro*. (A) Microwave heating curves of FCMP nanospheres (1.8 W, 5 min). (B) In the process of microwave irradiation, different concentrations of FCMP correspond to infrared (IR) thermal images at different times (1–5 min). (C) Microwave heating using different concentrations of FCMP (1, 3, 5, and 10 mg/mL). (D) Ultraviolet (UV) absorption spectra of GSH after scavenging by different amounts of FCMP nanospheres (0–6 mg), the UV excitation spectrum ranges from 405 to 500 nm. (E) UV spectra of GSH after scavenging by FCMP for different reaction times (10, 20, 40, and 80 min). (F) Percentage of residual GSH in cells after incubation with different concentrations of FCMP for 24 h.

ions, the bimetallic organic framework contains more catalytic sites that promote electron transfer, accelerate the excitation of H_2O_2, and produce •OH. Therefore, bimetallic MOFs are promising candidate materials for CDT. Electron spin resonance analysis experiments have proven that FCMP can catalyze the Fenton reaction of H_2O_2 to produce a •OH. By extending the reaction time, the ability to produce •OH was significantly enhanced (Fig. S5).

At the cellular level, we used FCMP nanospheres to generate ROS in four cell groups (control, FCMP, H_2O_2, and FCMP + H_2O_2). The dye DCFH-DA is oxidized by ROS and shows green fluorescence under a fluorescence microscope. As shown in Fig. 3J, the FCMP group produced weak green fluorescence, while the FCMP + H_2O_2 group exhibited bright green fluorescence. These observations demonstrate that FCMP catalyzes H_2O_2 decomposition to produce abundant ROS, further suppressing tumor cells in CDT.

3.5. Performance in internal and external MRI

It is well known that Fe ions can be used in MRI. We tested FCMP in MRI experiments both *in vivo* and *in vitro* (Fig. 4A). Upon increasing the concentration of FCMP nanospheres, the corresponding MRI signal gradually decreased. At the highest dose of 12 mg/mL, the magnetic resonance signal was so weak that it was barely detectable by the naked eye. This is significantly different from the results in the control group (deionized water only).

When FCMP was tested on tumor-bearing mice *in vivo*, the T_2 signal in tumor tissue gradually decreased with time after injection, compared to that before the injection. Six hours after FCMP injection, the T_2 signal decreased, indicating aggregation of nanoparticles at the tumor site. Through *in vivo* and *in vitro* MRI experiments, we verified that FCMP nanospheres could be used for real-time MRI, which provides a basis for further MRI-mediated tumor therapy.

3.6. In vitro degradation performance and cellular uptake

When FCMP was examined under TEM, we were surprised to find that the nanoparticle structure remained almost unchanged with the extension of reaction time at neutral pH. Conversely, the nanoparticles were gradually destroyed when incubated at acidic pH. After 24 h, the frame structure lost its original shape and completely collapsed (Fig. 4B). These observations revealed that the FCMP nanospheres have remarkable degradability in acidic environments. They first accumulate at the tumor site to enhance the therapy and then are degraded without long-term retention, indicating reduced toxicity and possible long-term application *in vivo* experiments. As shown in Fig. 4C, after incubation with tumor cells, FCMP nanospheres aggregated in the cytoplasm and nucleus. Magnified images further show that some nanospheres were gradually degraded to form a hollow structure, which verifies their biodegradability in the tumor cell environment. These results indicate that the multifunctional composite framework structure of FCMP can be taken up by tumor cells and biodegraded in the acidic conditions therein.

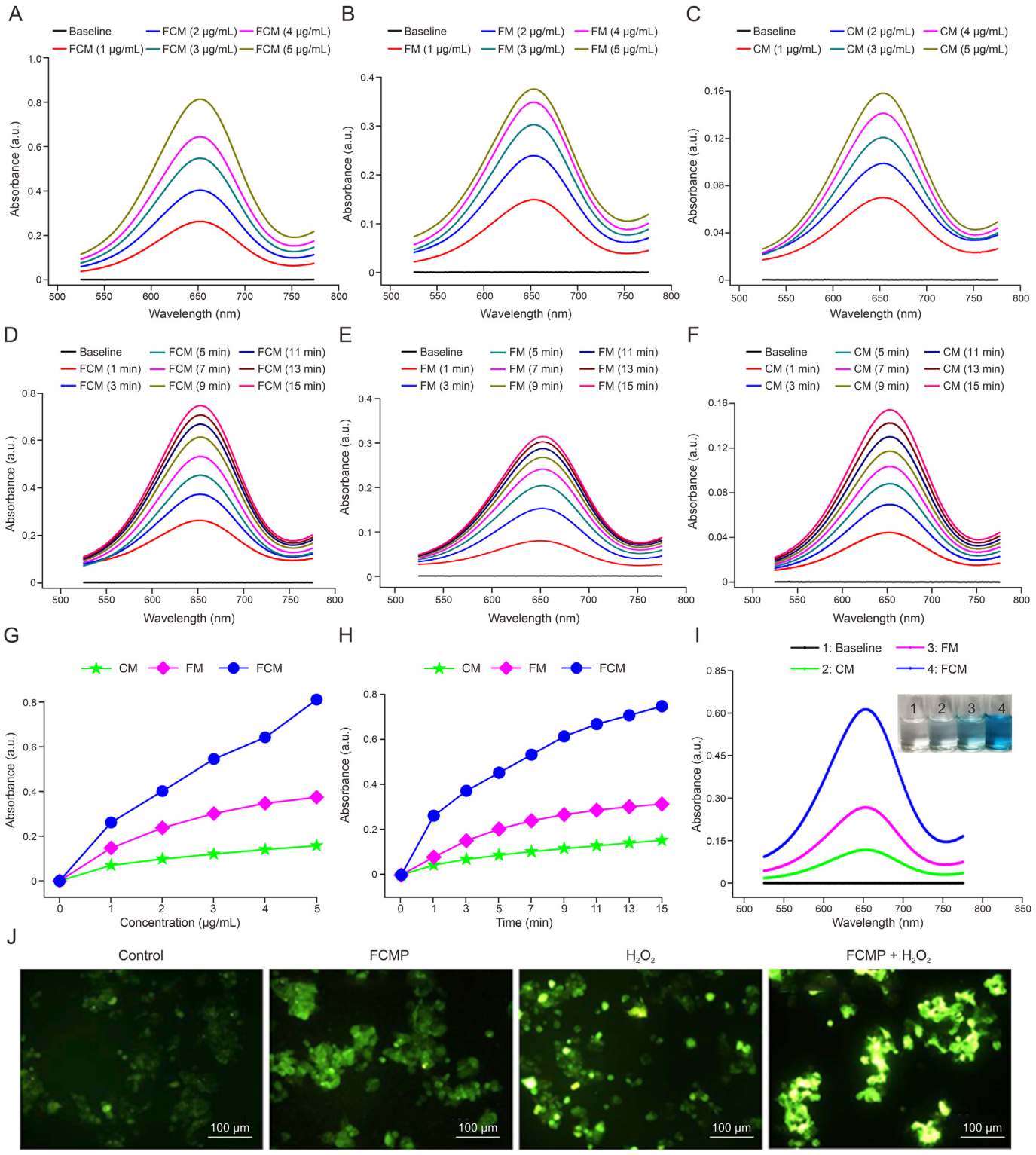

Fig. 3. *In vitro* performance of different metal-organic frameworks (MOFs) structure in chemodynamic therapy (CDT). (A-C) Ultraviolet (UV) absorption spectra of •OH produced by different particles at different concentrations (1–5 μg/mL): FeCuMOF (FCM) (A), FeMOF (FM) (B), and CuMOF (CM) (C). (D–F) UV absorption spectra of ·OH produced by different reaction times (1, 3, 5, 7, 9, 11, 13, and 15 min): FCM (D), FM (E), and CM (F). (G, H) Peak absorption at 652 nm for FCM, FM, and CM: different concentrations (G) and reaction times (H). (I) 3,3′,5,5′-tetramethylbenzidine (TMB) visible light absorption spectra of three MOFs materials (3 μg/mL) and the corresponding color changes. (J) Cell fluorescence image showing that FCM@polyethylene glycol (PEG) (FCMP) catalyzes H_2O_2 decomposition to produce reactive oxygen species (ROS) in four cell groups (control, FCMP, H_2O_2, and FCMP + H_2O_2). The dye 2,7-dichlorofluorescein acetoacetic acid (DCFH-DA) is oxidized by ROS and shows green fluorescence.

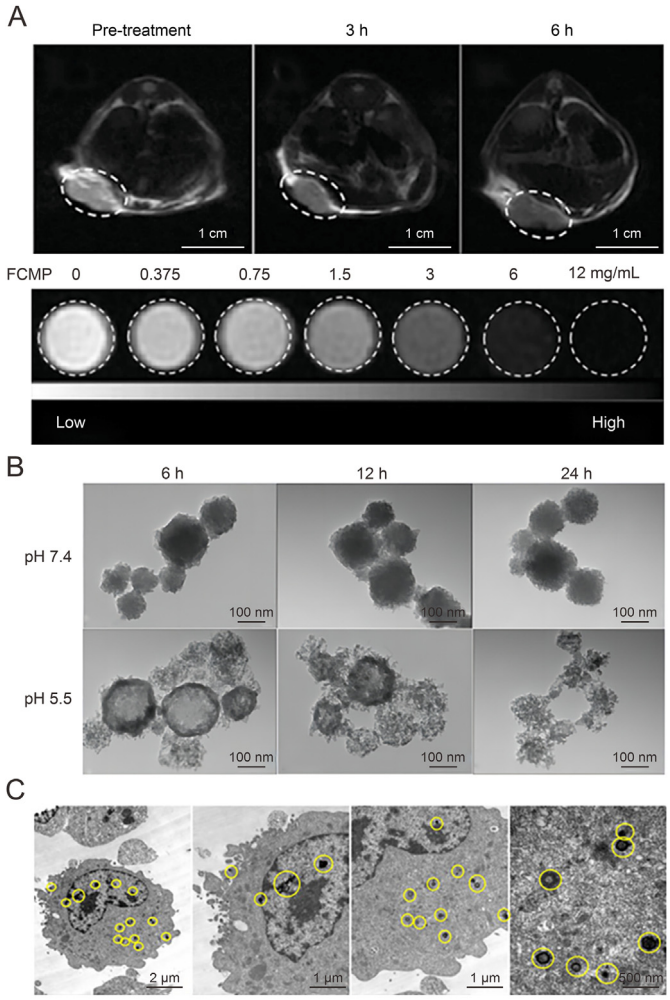

Fig. 4. FeCuMOF (FCM)@polyethylene glycol (PEG) (FCMP) *in vitro* and *in vivo* T_2 magnetic resonance imaging (MRI), degradation, and tumor cell uptake experiments. (A) T_2 MRI of tumor tissues at different times before and after injecting different amounts of FCMP in the tumor-bearing mouse and *in vitro* model. (B) Transmission electron microscopy (TEM) images of FCMP nanspheres after 6, 12, and 24 h at neutral pH (7.4) and in an acidic condition (pH 5.5). (C) TEM pictures of tumor cells after incubation with FCMP, showing cell uptake of the nanospheres.

3.7. In vivo and in vitro toxicity results

As shown in Fig. 5A, the survival rates of the three types of cells decreased slightly after treatment with FCMP in a dose-dependent manner. When the FCMP concentration was 50 μg/mL, the survival rates of L929, HepG2, and H22 cells were 97.2%, 92.8%, and 93.2%, respectively. When the concentration reached 200 μg/mL, the survival rates of the L929, HepG2, and H22 cells further decreased to 92.4%, 91.2%, and 87.8%, respectively. Overall, the FCMP nanospheres showed a low level of cytotoxicity.

We further verified the biosafety of FCMP through *in vivo* animal toxicity testing. Fig. S6A shows the daily body weight changes, and Figs. S6B–I display the blood analysis results (white blood cells (WBC), red blood cells (RBC), platelet (PLT), mean corpuscular volume (MCV), mean corpuscular hemoglobin (MCH), mean corpuscular hemoglobin concentration (MCHC), hemoglobin (HGB), and hematocrit (HCT)) for eyeball blood collected 14 days after treatment. Biochemical indices in the blood serum (alanine aminotransferase (ALT), aspartate aminotransferase (AST), blood urea nitrogen (BUN), and creatinine (CR)) are displayed in Fig. S7. The important organs (lungs, kidneys, heart, liver, and spleen) were subjected to H&E staining before observation (Fig. S8). At all injected concentrations, the FCMP nanospheres had no obvious effect on the weight and health status of the mice. The blood biochemistry and routine blood indicators were also within the normal range. The stained images did not reveal any abnormal changes in the organs. Acute toxicity *in vivo* experimental results were consistent with the *in vitro* results, further demonstrating the low biotoxicity of FCMP nanospheres.

3.8. In vitro tumor suppression performance in combined chemodynamic therapy and microwave hyperthermia

The tumor tissue is relatively enriched with H_2O_2, and our results showed that FCMP nanospheres catalyze H_2O_2 decomposition to produce •OH and ROS to enhance the efficacy of CDT. In our experimental results, the tumor cell viability first increased and then decreased upon increasing the H_2O_2 concentration. When the H_2O_2 concentration was less than 50 μM, the cell survival rate exceeded that of the control group. The cell survival rate at 50 μM was basically identical to that of the control, and it decreased at higher H_2O_2 concentrations (Fig. S9). Therefore, in subsequent experiments, we used 50 μM as the critical H_2O_2 concentration, as it was expected to neither promote nor hinder the proliferation of tumor cells.

To test the effects of combined MWTT and CDT on tumor cells *in vitro*, we incubated H22 cells with and without 50 μM H_2O_2 and/or FCMP for 24 h. Then, the cells were subjected to microwave irradiation. The results in Fig. 5B show that for each group, the cell survival rate decreased to various degrees upon extending the irradiation time. The most significant results were observed in the FCMP + H_2O_2 group, with cell survival rates of 78.23%, 72.78%, 44.21%, and 26.28% after irradiation for 0, 1, 3, and 5 min, respectively. This indicates that FCMP acts synergistically with H_2O_2 to kill tumor cells through two mechanisms: 1) acting as a sensitizer to induce hyperthermia under microwave irradiation and 2) catalyzing the decomposition of H_2O_2 to generate ROS.

3.9. Effect of FCMP on cell migration, apoptosis, and proliferation

We evaluated the effects of combined CDT and MWTT in the presence of FCMP on the migration, apoptosis, and proliferation of tumor cells. There were six groups: control, FCMP, H_2O_2, microwave, FCMP + microwave, and FCMP + microwave + H_2O_2. Fig. S10 shows the cell survival rates detected by the MTT method. In the transwell cell migration experiment, the FCMP and H_2O_2 groups showed slightly inhibited cell migration compared to that of the control, FCMP + microwave showed obvious inhibition, and FCMP + microwave + H_2O_2 completely stopped tumor cell migration (Fig. 5C). In the apoptosis experiment, each cell group showed some degree of apoptosis, and the apoptosis rate was higher when microwave irradiation was applied. Among them, the FCMP + microwave + H_2O_2 group reached an apoptotic cell ratio of 53.2%, which was 20.46-fold higher than that of the control group (Fig. 5D), indicating that FCMP combined with microwave treatment significantly promoted cell apoptosis. A cell EdU proliferation assay was used to analyze apoptosis at the cellular level by reacting specific fluorescent dyes with thymidine analogs of EdU, which enter DNA molecules under synthesis to report on DNA replication activity. In Fig. 5E, the cells of the control group showed significant red fluorescence, while the FCMP + microwave + H_2O_2 group hardly showed any, further proving almost complete inhibition of cell proliferation in the FCMP + microwave + H_2O_2 group. These results indicate that when used in combined CDT and MTT therapies, FCMP could inhibit tumor cell migration, promote cell

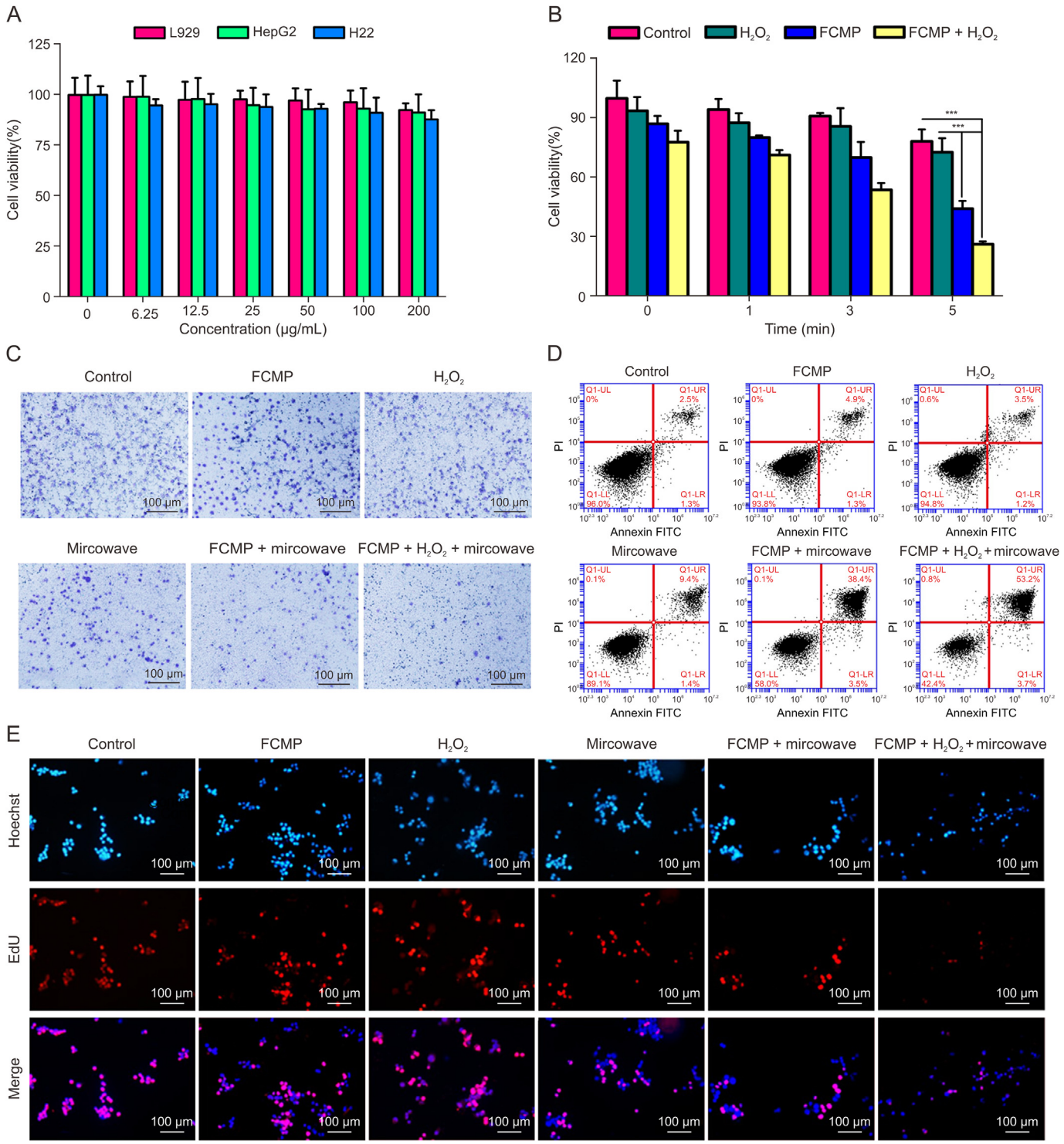

Fig. 5. Biosafety evaluation of FeCuMOF (FCM)@polyethylene glycol (PEG) (FCMP) nanospheres *in vivo* and *in vitro*. (A) Effects of FCMP concentration on the survival rates of normal cells (L929) and cancer cells (HepG2 and H22), as detected with methylthiazolyldiphenyl-tetrazolium (MTT) assay. (B) Cell survival ratios in the control, FCMP, H_2O_2, and FCMP + H_2O_2 groups after microwave treatment for 1, 3, and 5 min. (C) Effect of FCMP nanspheres on the migration of tumor cells. (D) Cell apoptosis detected by flow cytometry after the same treatment as Fig. 5C. (E) Cell proliferation ability as evaluated by performing the 5-ethynyl-2′-deoxyuridine (EdU) test. $^{***}P < 0.001$. PI: propidium iodide; FITC: fluorescein isothiocyanate; UL: upper left; UR: upper right; LL: lower left; LR: lower right.

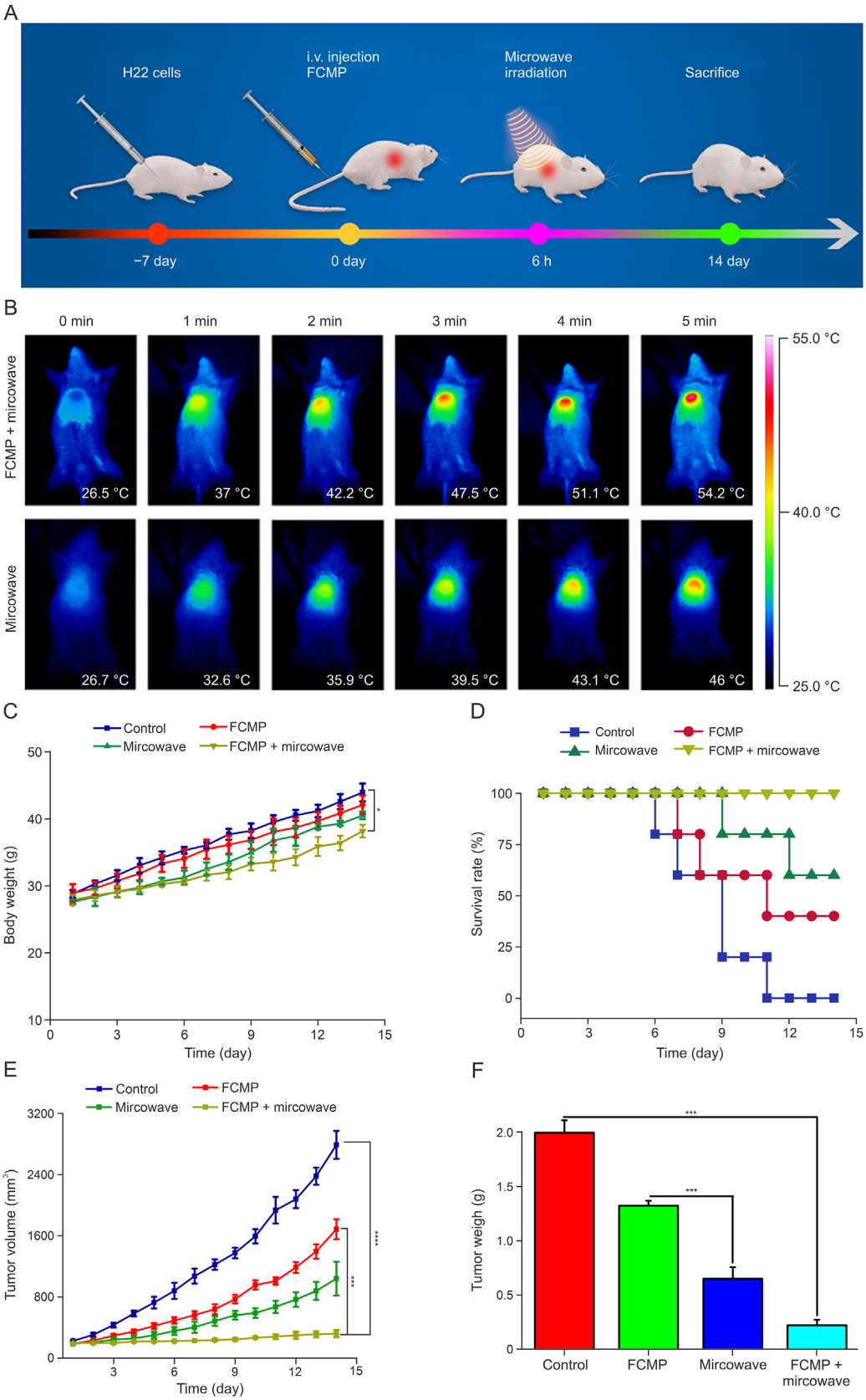

Fig. 6. Evaluation of tumor inhibition of FeCuMOF (FCM)@polyethylene glycol (PEG) (FCMP) in tumor-bearing mice. (A) Operation flow chart of tumor inhibition experiment *in vivo* in tumor-bearing mice. (B) Infrared (IR) thermography under local microwave irradiation on tumor-bearing mice from the FCMP + microwave and microwave groups (1.8 W, 5 min). (C) The change curves of mice weight during treatment cycle (1–14 days). (D) Survival rate of tumor-bearing mice during treatment. (E) Tumor volume changes during the experimental period. (F) Tumor weight in the mice 14 days after treatment. $^{*}P < 0.05$, $^{***}P < 0.001$, and $^{****}P < 0.0001$.

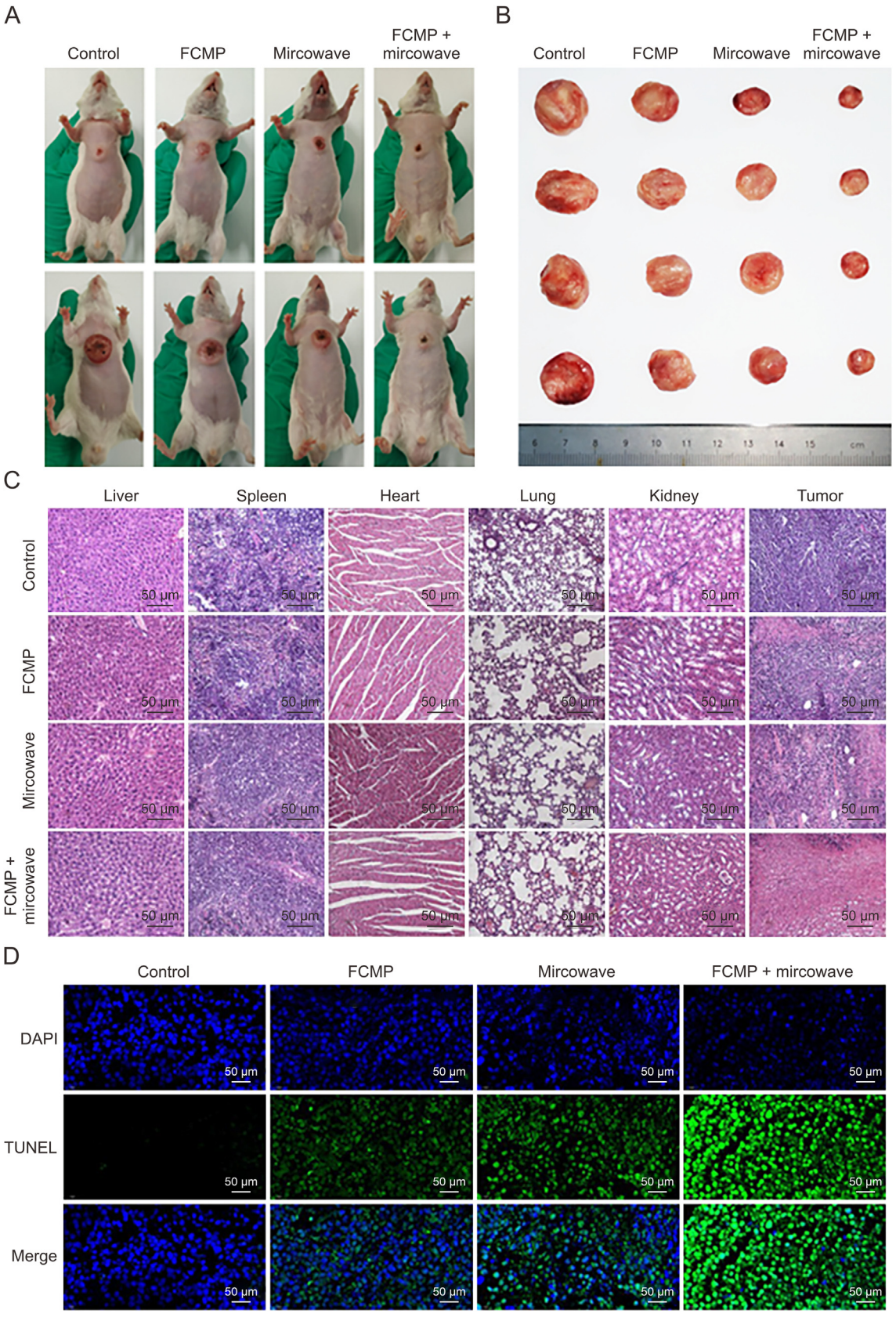

Fig. 7. Evaluation of tumor inhibition of FeCuMOF (FCM)@polyethylene glycol (PEG) (FCMP) in tumor-bearing mice at 14 days after treatment. (A) Photos of male mice with tumors in each group at 0 and 14 days after treatment. (B) Photographs of excised tumor tissue at 14 days after treatment. (C) Hematoxylin and eosin (H&E)-stained tumor tissue and important organs at 14 days after treatment. (D) Terminal deoxynucleotidyl transferase dUTP nick-end labeling (TUNEL) apoptosis staining image in tumor tissues for each group. DAPI: 4',6-diamidino-2-phenylindole.

apoptosis, and hinder cell proliferation, all of which contribute to tumor suppression.

3.10. In vivo performance of tumor inhibition by FCMP

Combined with the above *in vitro* experimental results, we established a tumor-bearing mouse model and further evaluated the tumor suppressive effect of FCMP nanospheres on tumor-bearing mice *in vivo* (Fig. 6A). The mice were evenly divided into four groups: control, FCMP, microwave, and FCMP + microwave. Extending the microwave irradiation time led to a significantly higher temperature at the tumor site compared to that in adjacent tissues, and the FCMP + microwavegroup showed a much greater temperature elevation than the microwave group (Fig. 6B). In the IR thermal images, the color became brighter with irradiation time, and after 5 min of irradiation, the tumor site in the FCMP + microwave group appeared crimson. From these findings, we concluded that the FCMP nanospheres achieved significant heating under microwave irradiation at the tumor site.

After treatment, the mice in each group generally showed an upward trend in body weight: that of the control group increased the fastest, those of the FCMP and microwave groups increased at similar moderate rates, and that of the FCMP + microwave group increased most slowly (Fig. 6C), further reflecting different rates of tumor growth in the mice. The survival curve of the mice is shown in Fig. 6D. Fourteen days after treatment, all mice in the control group had died, and 40%, 60%, and 100% of the mice survived in the FCMP, microwave, and FCMP + microwave groups, respectively. In terms of tumor volume, the FCMP and microwave groups showed an upward trend, the control group showed the greatest increase, and the FCMP + microwave group presented no increase (Fig. 6E). After treatment, the tumor tissues and important organs of the mice were harvested and weighed. The weight of the tumor tissues was ranked as follows: control > FCMP > microwave > FCMP + microwave (Fig. 6F). Notably, the tumor weight in the control group was 9.0-fold higher than that of the FCMP + microwave group, demonstrating that the FCMP nanospheres have a significant tumor growth-inhibiting effect under microwave irradiation.

Fig. 7A shows the changes in tumor size before and 14 days after treatment in each group. Photographs of tumor tissues harvested 14 days after treatment are displayed in Fig. 7B. The difference between the control and FCMP + microwave groups was obvious. The analysis of the H&E-stained tumor tissues and organs (Fig. 7C) showed that the tumor cells in the control group were basically undamaged, some of them were damaged in the FCMP and microwave groups (with more damage in the microwave group), and those in the FCMP + microwave group were almost completely destroyed. Meanwhile, the major organs showed no significant damage or histological abnormalities, indicating that the FCMP nanocomposite framework has good biocompatibility and sufficient efficacy in inhibiting tumors. Finally, we performed apoptosis TUNEL fluorescence staining on the excised tumor tissues to verify apoptosis in the different groups. Fig. 7D shows the green fluorescence corresponding to TUNEL. The fluorescence was absent in the control group, weak in the FCMP and microwave groups, and bright in the FCMP + microwave group. The merged image more intuitively illustrates the apoptotic cells in each group. These *in vivo* results confirm that the FCMP nanomaterial has a good tumor-inhibiting effect in combination with CDT-MWTT.

4. Conclusions

A new biodegradable Fe−Cu bimetallic organic framework FCMP was synthesized by hydrothermal method as a microwave sensitizer for tumor therapy. We found that FCMP generated a significant amount of heat under microwave irradiation. It also acted as a nanozyme to produce •OH from H_2O_2, and the amounts of •OH produced were 2.17- and 5.12-fold higher than those for single-metallic FM and CM, respectively, under the same reaction conditions. Furthermore, FCMP clears GSH in tumor cells. Therefore, FCMP indirectly enhances the efficacy of chemodynamic therapy and allows its combination with microwave-induced hyperthermia for treating tumors. In addition, FCMP demonstrated the ability for *in vivo* and *in vitro* MRI, excellent biocompatibility, and favorable biodegradation performance. Therefore, FCMP may be employed for accurate positioning in real-time MRI, coordinating the two treatment modalities mentioned above, and achieve high efficacy for the inhibition and treatment of tumors. The findings of our study represent a breakthrough for integrating both the diagnosis and treatment of tumors and provide a reference for developing new microwave sensitizers.

CRediT author statement

Xinyang Zhu: Methodology, Data curation, Validation, Investigation, Writing - Original draft preparation; **Chao He:** Methodology, Resources, Writing - Reviewing and Editing; **Longfei Tan:** Methodology, Conceptualization; **Xun Qi:** Conceptualization, Formal analysis; **Meng Niu:** Writing - Reviewing and Editing; **Xianwei Meng:** Conceptualization, Methodology, Resources; **Hongshan Zhong:** Resources, Funding acquisition, Writing - Reviewing and Editing, Supervision.

Declaration of competing interest

The authors declare that there are no conflicts of interest.

Acknowledgments

We thank Prof. Xiangling Ren, Mr. Zengzhen Chen, and Ms. Qiong Wu from the Technical Institute of Physics and Chemistry, University of Chinese Academy of Sciences and Mr. Dongqi Li, Mr. Qiaozheng Wang from the first Clinical College of China Medical University for helping us complete the experiments. This work was supported by the National Key R&D Program of China (Grant No.: 2018YFC0115500), the National Natural Science Foundation of China (Grant No.: U21A20378), Liaoning Revitalization Talents Program, China (Grant No.: XLYC1802098), the Natural Science Foundation of Shaanxi Provincical Department of Education, China (Grant No.: 21JK0593), and the Key Research and Development Plan of Science and Technology Department of Xianyang City, China (Grant No.: L2023-ZDYF-SF-054).

Appendix A. Supplementary data

Supplementary data to this article can be found online at https://doi.org/10.1016/j.jpha.2024.02.006.

References

[1] X. Li, W. Yao, Y. Yuan, et al., Targeting of tumour-infiltrating macrophages via CCL2/CCR2 signalling as a therapeutic strategy against hepatocellular carcinoma, Gut 66 (2017) 157−167.
[2] J. Qi, W. Li, K. Lu, et al., pH and thermal dual-sensitive nanoparticle-mediated synergistic antitumor effect of immunotherapy and microwave thermotherapy, Nano Lett. 19 (2019) 4949−4959.
[3] T. Zhou, X. Liang, P. Wang, et al., A hepatocellular carcinoma targeting nanostrategy with hypoxia-ameliorating and photothermal abilities that, combined with immunotherapy, inhibits metastasis and recurrence, ACS Nano 14 (2020) 12679−12696.
[4] M. Chang, Z. Hou, M. Wang, et al., Single-atom Pd nanozyme for ferroptosis-boosted mild-temperature photothermal therapy, Angew. Chem. Int. Ed. Engl. 60 (2021) 12971−12979.

[5] M. Dunne, J.C. Evans, M.W. Dewhirst, et al., The integration of hyperthermia and drug delivery, Adv. Drug Deliv. Rev. 163-164 (2020) 1–2.
[6] T. Li, Q. Wu, W. Wang, et al., MOF-derived nano-popcorns synthesized by sonochemistry as efficient sensitizers for tumor microwave thermal therapy, Biomaterials 234 (2020), 119773.
[7] X. Ma, X. Ren, X. Guo, et al., Multifunctional iron-based metal-organic framework as biodegradable nanozyme for microwave enhancing dynamic therapy, Biomaterials 214 (2019), 119223.
[8] Q. Wu, N. Xia, D. Long, et al., Dual-functional supernanoparticles with microwave dynamic therapy and microwave thermal therapy, Nano Lett. 19 (2019) 5277–5286.
[9] S. Li, Z. Chen, L. Tan, et al., MOF@COF nanocapsule for the enhanced microwave thermal-dynamic therapy and anti-angiogenesis of colorectal cancer, Biomaterials 283 (2022), 121472.
[10] J. Liu, L. Zhang, J. Lei, et al., Multifunctional metal-organic framework nanoprobe for cathepsin B-activated cancer cell imaging and chemo-photodynamic therapy, ACS Appl. Mater. Interfaces 9 (2017) 2150–2158.
[11] H. Min, J. Wang, Y. Qi, et al., Biomimetic metal-organic framework nanoparticles for cooperative combination of antiangiogenesis and photodynamic therapy for enhanced efficacy, Adv. Mater. 31 (2019), e1808200.
[12] L. Su, Q. Wu, L. Tan, et al., High biocompatible ZIF-8 coated by ZrO_2 for chemo-microwave thermal tumor synergistic therapy, ACS Appl. Mater. Interfaces 11 (2019) 10520–10531.
[13] V. Guillerm, M. Eddaoudi, The importance of highly connected building units in reticular chemistry: Thoughtful design of metal-organic frameworks, Acc. Chem. Res. 54 (2021) 3298–3312.
[14] T. Luo, G.T. Nash, Z. Xu, et al., Nanoscale metal-organic framework confines zinc-phthalocyanine photosensitizers for enhanced photodynamic therapy, J. Am. Chem. Soc. 143 (2021) 13519–13524.
[15] Y.-Y. Xue, X.-Y. Bai, J. Zhang, et al., Precise pore space partitions combined with high-density hydrogen-bonding acceptors within metal-organic frameworks for highly efficient acetylene storage and separation, Angew. Chem. Int. Ed. Engl. 60 (2021) 10122–10128.
[16] X. Sun, B. Niu, Q. Zhang, et al., MIL-53-based homochiral metal-organic framework as a stationary phase for open-tubular capillary electrochromatography, J. Pharm. Anal. 12 (2022) 509–516.
[17] D. Sun, S. Zhou, W. Gao, What went wrong with anticancer nanomedicine design and how to make it right, ACS Nano 14 (2020) 12281–12290.
[18] Z. Fan, H. Liu, Y. Xue, et al., Reversing cold tumors to hot: An immunoadjuvant-functionalized metal-organic framework for multimodal imaging-guided synergistic photo-immunotherapy, Bioact. Mater. 6 (2021) 312–325.
[19] J. Xu, X. Cheng, L. Tan, et al., Microwave responsive nanoplatform via P-selectin mediated drug delivery for treatment of hepatocellular carcinoma with distant metastasis, Nano Lett. 19 (2019) 2914–2927.
[20] M. Izci, C. Maksoudian, B.B. Manshian, et al., The use of alternative strategies for enhanced nanoparticle delivery to solid tumors, Chem. Rev. 121 (2021) 1746–1803.
[21] L.-H. Fu, Y. Wan, C. Qi, et al., Nanocatalytic theranostics with glutathione depletion and enhanced reactive oxygen species generation for efficient cancer therapy, Adv. Mater. 33 (2021), e2006892.
[22] S. Dong, Y. Dong, T. Jia, et al., GSH-depleted nanozymes with hyperthermia-enhanced dual enzyme-mimic activities for tumor nanocatalytic therapy, Adv. Mater. 32 (2020), e2002439.
[23] Y. Dong, S. Dong, B. Liu, et al., 2D piezoelectric Bi_2MoO_6 nanoribbons for GSH-enhanced sonodynamic therapy, Adv. Mater. (2021), e2106838.
[24] Z. Ren, S. Sun, R. Sun, et al., A metal-polyphenol-coordinated nanomedicine for synergistic cascade cancer chemotherapy and chemodynamic therapy, Adv. Mater. 32 (2020), e1906024.
[25] T. He, C. Jiang, J. He, et al., Manganese-dioxide-coating-instructed plasmonic modulation of gold nanorods for activatable duplex-imaging-guided NIR-II photothermal-chemodynamic therapy, Adv. Mater. 33 (2021), e2008540.
[26] Y. Zhou, S. Fan, L. Feng, et al., Manipulating intratumoral Fenton chemistry for enhanced chemodynamic and chemodynamic-synergized multimodal therapy, Adv. Mater. 33 (2021), e2104223.
[27] C. Fu, H. Zhou, L. Tan, et al., Microwave-activated Mn-doped zirconium metal-organic framework nanocubes for highly effective combination of microwave dynamic and thermal therapies against cancer, ACS Nano 12 (2018) 2201–2210.
[28] B. Halliwell, A. Adhikary, M. Dingfelder, et al., Hydroxyl radical is a significant player in oxidative DNA damage *in vivo*, Chem. Soc. Rev. 50 (2021) 8355–8360.
[29] C. Cao, H. Zou, N. Yang, et al., Fe_3O_4/Ag/Bi_2MoO_6 photoactivatable nanozyme for self-replenishing and sustainable cascaded nanocatalytic cancer therapy, Adv. Mater. 33 (2021), e2106996.
[30] J. Wang, Y. Jia, Q. Wang, et al., An ultrahigh-field-tailored T_1-T_2 dual-mode MRI contrast agent for high-performance vascular imaging, Adv. Mater. 33 (2021), e2004917.